Electrochimica Acta 104 (2013) 518–525

Contents lists available at SciVerse ScienceDirect

Electrochimica Acta

journal homepage: www.elsevier.com/locate/electacta

Anodic oxidation of zirconium in silicate solutions

Wojciech Simka[a,*], Maciej Sowa[a], Robert P. Socha[b], Artur Maciej[a], Joanna Michalska[c]

[a] Faculty of Chemistry, Silesian University of Technology, B. Krzywoustego Street 6, 44-100 Gliwice, Poland
[b] Jerzy Haber Institute of Catalysis and Surface Chemistry PAS, Niezapominajek Street 8, 30-239 Krakow, Poland
[c] Faculty of Materials Science and Metallurgy, Silesian University of Technology, Krasińskiego Street 8, 40-019 Katowice, Poland

ARTICLE INFO

Article history:
Received 28 August 2012
Received in revised form 7 October 2012
Accepted 27 October 2012
Available online 2 November 2012

Keywords:
Zirconium
Plasma electrolytic oxidation
Corrosion
Silicate solutions

ABSTRACT

Herein, a study of the surface modification of zirconium by anodic oxidation is reported. The oxidation process was carried out in a solution containing K_2SiO_3 and KOH. The anodization was conducted at voltages of 100, 200 and 400 V. It was found that the morphology of the surface did not change during the oxidation of the zirconium at 100 and 200 V. The application of 400 V resulted in the incorporation of silicon into the formed oxide layer and a significant modification of the surface morphology. The obtained coatings are typical of coating produced during an electrolytic plasma oxidation process and contain a considerable amount of silicon. The anodic oxidation of zirconium leads to a significant improvement in the corrosion resistance of the material in the presence of Ringer's physiological solution.

1. Introduction

Implants made of metals or alloys are widely used in medicine. These materials cannot be introduced into the human body without a proper surface treatment. A modification must be performed to provide the appropriate functional properties on the surface of the implants. Biologically active or non-active surfaces can be formed by electrochemical methods that are often used during metal biomaterials production. The electrochemical processes used in implant production include: electrolytic etching, electrolytic polishing, anodic oxidation, electrophoretic deposition and cathodic deposition. The electrolytic polishing process is used for the production of very smooth and tension-free surfaces. Moreover, it results in an increase in the corrosion resistance of treated elements [1]. The effects obtained in the process can be improved by the application of a magnetic field [2,3]. Electrophoretic and cathodic depositions are used for the formation of layers, e.g., apatite layers on titanium implants that increase their bioactivity [4,5]. The anodic oxidation process is commonly used for the treatment of biomaterials made of titanium and its alloys, as well magnesium, niobium, tantalum and zirconium [6,7]. It also can be used for the formation of thin oxide layers that considerably improve the corrosion resistance of the implants [8–10]. A particular type of process is the so-called plasma electrolytic oxidation (PEO) or micro-arc oxidation (MAO), which proceed above the oxide layer breakdown potential [11]. A number of physical and chemical phenomena occur during this type of oxidation. These phenomena make it possible to obtain a treated surface coating of a ceramic that is enriched in the components present in the anodizing solution [12–15]. The coatings exhibit very good tribological properties, good corrosion resistance and improve the osseointegration of the coated biomaterials [16].

Commercially pure Ti and Ti–6Al–4V extra low interstitial (ELI) are the most commonly used titanium materials for implant applications. Although Ti–6Al–4V was originally developed for aerospace applications, its high corrosion resistance and excellent biocompatibility led to its entry into the biomedical industry [17]. Although titanium and its alloys, mainly Ti–6Al–4V, have excellent corrosion resistance and biocompatibility, some concerns have been raised about to the release of aluminum and vanadium from the Ti–6Al–4V alloy. Both Al and V ions have been associated with long-term health problems, such as Alzheimer disease, neuropathy and ostemomalacia [18]. In addition, vanadium is toxic both in its elemental state and as the V_2O_5 oxide, which is present at the surface [19,20]. Further, titanium has poor shear strength, making it less desirable for bone screws, plates and similar applications. Titanium also tends to undergo severe wear when it is rubbed between itself and other metals [21]. Titanium-based alloys with a high coefficient of friction can lead to the formation of wear debris that produce an inflammatory reaction, causing pain and the loosening of implants due to osteolysis [22]. The growing requirements for long-term implants, as well as doubts regarding the bioinertness of titanium alloys containing vanadium have contributed to the growing number of investigations of vanadium-free titanium alloys. Among the studied alloys, the most promising metallic biomaterials include [17] titanium–aluminum–niobium

* Corresponding author.
E-mail address: wojciech.simka@polsl.pl (W. Simka).

0013-4686/$ – see front matter © 2012 Elsevier Ltd. All rights reserved.
http://dx.doi.org/10.1016/j.electacta.2012.10.130

(Ti–6Al–7Nb), titanium–niobium–zirconium (Ti–13Nb–13Zr), titanium–niobium–tantalum–zirconium (Ti–29Nb–13Ta–4.5Zr) and titanium–niobium (Ti–50Nb). Instead of the harmful aluminum and vanadium, other metals such as zirconium, niobium and tantalum are predominantly used because these alloys are much more resistant to corrosion in the presence of bodily fluids than other alloys [23–30]. Previous studies have shown that pure Ti, Nb, and Zr metals and alloys exhibit excellent corrosion resistance in chloride, which is related to the presence of a stable and protective oxide film on the surface (mainly TiO_2, Nb_2O_5 and ZrO_2) [28,31]. The addition of Nb and Zr increases the thermodynamic and kinetic stability of Ti in the alloy and thus reduces the dissolution rate of Ti [25]. Moreover, the oxide Nb_2O_5 has a more negative heat of formation than Al_2O_3 and V_2O_5, and Zr and Nb ions have lower solubility than Al and V ions in aqueous media [26,29].

Silicon (Si) is an essential element for the normal growth and development of bone and connective tissues [32,33]. The role of Si as an essential element for higher biological organisms was discovered through deficiency studies [34]. In recent years, increasing evidence supports the hypothesis that the presence of Si contributes to the enhanced bioactivity of some bioactive glasses and ceramics and significantly increases the up-regulation of osteoblast proliferation and gene expression [35]. Si-containing calcium phosphate ceramics were widely investigated and proven to be more bioactive and favorable for the attachment and spread of osteoblasts [33]. The incorporation of Si into conventional films by PEO is a promising approach for introducing certain elements into the film to enhance its bioactivity and thus favor skeleton formation.

Herein, the results of plasma electrolytic oxidation of pure zirconium for the preparation of vanadium-free titanium alloys are reported. The process was carried out in aqueous solutions of potassium silicate and potassium hydroxide. The morphology, chemical composition as well as the corrosion resistance of surface-modified zirconium were evaluated.

2. Materials and methods

Pure zirconium (BIMO Metals, Wrocław, Poland) samples in the shape of a plate with dimensions of 10 mm × 10 mm were used in this study. The samples were polished with #320 and #600 abrasive paper and cleaned for 5 min in an ultrasonic wash in 2-propanol and deionized water. The pretreatment of samples was conducted as follows: polishing with abrasive paper of 600 granulation, etching in a solution containing H_2SO_4 (4 mol dm^{-3}) and HF (1 mol dm^{-3}) for 1 min, rinsing in distilled water and cleaning ultrasonically for 5 min (sample Zr).

After the etching process, the samples were oxidized anodically in a bath containing potassium hydroxide (KOH – 5 g dm^{-3}) and potassium silicate (K_2SiO_3; different concentration). The anodization was carried out at a current density of 0.1 A dm^{-2} for 5 min. The sample labels and treatment conditions are provided in Table 1. After anodization, the samples were rinsed with distilled water and cleaned in an ultrasonic bath with 2-propanol and deionized water. A DC power supply (PWR800H, Kikusui, Japan) was used for the anodization reaction, in which the zirconium specimen served as the anode and a titanium plate served as the cathode.

The morphology and the cross sectional and chemical composition of the anodic layer formed on the surface were examined using a scanning electron microscope (SEM, Hitachi S-3400N, accelerating voltage = 25 kV) equipped with an energy-dispersive X-ray spectrometer (EDX, Thermo Noran).

The X-ray photoelectron spectroscopy (XPS) measurements were performed in an ultrahigh vacuum (3×10^{-10} mbar) system equipped with a hemispherical analyzer (SES R4000, Gammadata Scienta). An un-monochromatic Mg Kα X-ray source of incident energy of 1253.6 eV was applied to generate core excitations. The energy resolution of the system, measured as a full width at half maximum for an Ag 3d5/2 excitation line, was 0.9 eV. The energy scale of the analyzer was calibrated according to ISO 15472:2001, and the energy scale of the acquired spectra was calibrated for a maximum C 1s core excitation at the electron binding energy (BE) of 285 eV. The analytical depth for the measured samples (approximated as SiO_2 layers) was 10.4 nm.

The roughness (Ra parameter) of the samples was measured using a Mitutoyo Surftest SJ-301 profilometer according to ISO 4287:1997. The Ra parameter is the arithmetic mean of the sum of roughness profile values:

$$\mathrm{Ra} = \frac{1}{l}\int_0^l \left|Z(x)\right| dx, \quad (1)$$

where $|Z(x)|$ is the absolute ordinate value inside the elementary measuring length and l is the elementary length in the x direction (average line) used to determine the unevenness of the profile.

The corrosion resistance of the zirconium samples was investigated in the presence of Ringer's simulated body fluid, which is composed of 8.6 g dm^{-3} NaCl, 0.3 g dm^{-3} KCl, and 0.48 g dm^{-3} $CaCl_2 \cdot 6H_2O$ (Baxter, USA). The main components of the research apparatus included a standard two-chamber electrolysis cell with three electrodes: a working electrode, a platinum auxiliary electrode and a Haber–Luggin capillary with a reference electrode (saturated calomel electrode – SCE). The electrolysis cell was powered by a PARSTAT 4000 potentiostat operated by the Versa Studio software. The study included the following measurements: (a) recording the open-circuit potential (E_{OCP}) as a function of time, (b) determining the $\log i = f(E)$ curve in the potential range of E_{OCP} −20 mV to E_{OCP} +20 mV ($dE\,dt^{-1}$ = 1 mV s^{-1}), which provides information about: (i) the corrosion potential E_{CORR}, mV, (ii) the corrosion current density i_{CORR}, nA cm^{-2}, and (iii) the polarization resistance R_p, kΩ cm^2, and (c) recording the cyclic polarization curve (CV) in the potential range from E_{OCP} −0.1 V to 3 V ($dE\,dt^{-1}$ = 10 mV s^{-1}).

All solutions were prepared using analytical grade reagents manufactured by POCh Gliwice, Poland. Deionized water was obtained from the Millipore Milli-Q system.

3. Results and discussion

The surface of the polished and etched zirconium exhibits the expected morphology following such a treatment (Fig. 1). The

Table 1
The sample labels, treatment condition, Zr/Si surface atomic ratio, roughness, and thickness of the samples; KOH – 5 g dm^{-3}.

Sample	K_2SiO_3, mol dm^{-3}	U, V	Zr/Si surface atomic ratio	Ra, μm	Thickness, μm
Zr-ANO-0.5-100	0.5	100	51.63	0.24	0.32–0.38
Zr-ANO-0.5-200		200	29.30	0.26	0.56–0.76
Zr-ANO-0.5-400		400	0.085	3.70	10.2–18.0
Zr-ANO-0.1-400	0.1	400	12.42	1.46	5.16–5.56
Zr-ANO-1.0-400	1.0		0.005	4.09	41.3–70.6

Zr Ra = 0.23 μm.

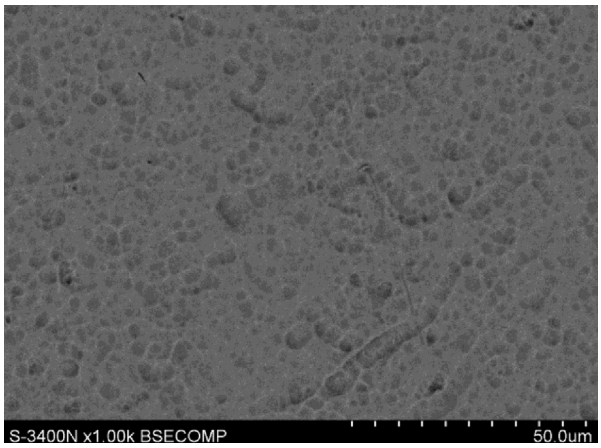

Fig. 1. The SEM image of the etched zirconium in the solution containing H_2SO_4 (4 mol dm^{-3}) and HF (1 mol dm^{-3}).

Ra roughness parameter of the etched zirconium was 0.23 μm (Table 1, Fig. 2). The etched zirconium was then anodically oxidized under different parameters. The anodic oxidation performed in a solution containing 0.5 mol dm^{-3} K_2SiO_3 at a voltage of 100 V did not affect the surface morphology of zirconium samples (Fig. 3). The roughness was close to the Ra parameter of the substrate of 0.24 μm (Table 1 and Fig. 2). The EDX analysis demonstrated the presence of zirconium, oxygen and silicon on the surface of sample Zr-ANO-0.5-100 (spectra not shown). The presence of oxygen in the EDX spectra suggests that ZrO_2 and SiO_2 were observed on the surface of zirconium samples. The Zr/Si atomic ratio, calculated from the EDX data, was 51.63. This value indicates a low amount of silicon in the coating. The obtained coating was compact and uniformly covered the specimen. As expected for a barrier type anodic coating, it exhibited a thickness of 320–380 nm. The coating was formed below the potential when the oxide layer breakdown takes place (Fig. 3) [36]. A further increase in the voltage to 200 V did not influence the surface appearance (Zr-ANO-0.5-200 sample, Fig. 4). The Zr/Si atomic ratio decreased to 29.30, confirming an increase in the silicon content of the coating (Table 1). Cheng et al. investigated the plasma electrolytic oxidation of titanium in solutions containing calcium, silicon and sodium [37]. Silicon in the form of SiO_2 was incorporated into the oxide layer formed on titanium at a voltage of 200 V. The formed coating was also a barrier type coating with a thickness in the range of 560–760 nm (Fig. 4, Table 1). Based on the thickness analysis of the coatings formed at 100 and 200 V, it can be concluded that the change in the thickness of the coating in relation to the applied voltage is linear and averages 3.4 nm V^{-1} for this voltage range and a current density of 100 mA cm^{-2}.

The change in anodizing voltage over the course of the zirconium oxidation at the maximum terminal voltage (400 V) is shown in Fig. 5. The curves are typical of a PEO process [15], wherein three segments can be distinguished: (1) a fast and linear increase in the voltage from 0 to 230 V, (2) a decrease in the rate of voltage increase (from approximately 230 to approximately 300 V) and the breakdown of the zirconium oxide layer appears above the voltage of 230 V, and (3) an intense discharge of the surface of zirconium and the lowest change in the rate. Increasing the potassium silicate concentration in the solution resulted in an increase in the rate in the first rectilinear segment of 9.0, 9.8, and 12.4 V s^{-1} for K_2SiO_3 concentrations of 0.1, 0.5, and 1.0 mol dm^{-3}, respectively. The roughness of the surface also exhibited an increase with increasing voltage (Fig. 2). The roughness factors were 1.46, 3.70, and 4.09 μm for K_2SiO_3 concentrations of 0.1, 0.5 and, 1.0 mol dm^{-3}, respectively (Table 2).

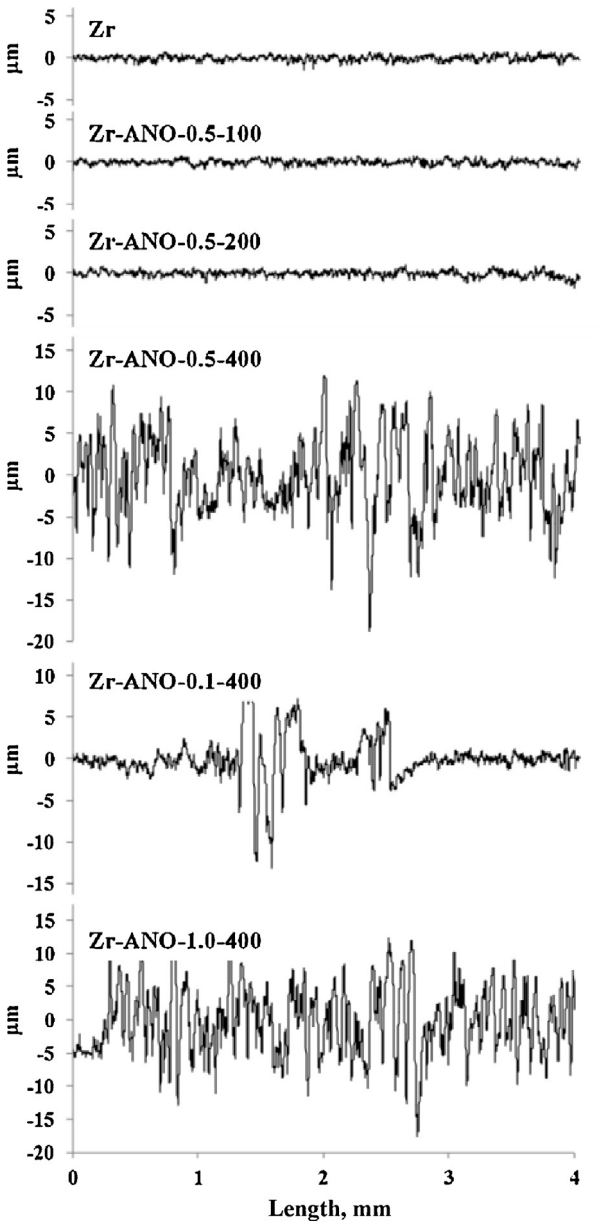

Fig. 2. The surface profiles of the etched zirconium and zirconium anodized at different conditions (Zr-ANO-x-y samples).

Increasing the voltage during the oxidation in a solution of silicate and potassium hydroxide fundamentally influences the morphology and chemical composition of the obtained oxide layer (Zr-ANO-x-400 sample; Figs. 6–9). An increase in the potassium silicate concentration in the solution increases the silicon content of the oxide layer. The calculated Zr/Si atomic ratios were 12.42, 0.085, and 0.005 for K_2SiO_3 concentrations of 0.1, 0.5, and

Table 2
Parameters of the deconvoluted O 1s, Si 2p, and Zr 3d core excitations for Zr-ANO-0.5-400 sample.

Core excitation	Component	BE (eV)	%	Assignation
O	A	530.5	33.8	O—metal
1s	B	532.4	56.7	O—Si
	C	533.5	9.5	O—C, H_2O
Si $2p_{3/2}$	A	102.8	100.0	Si—O
Zr	A	182.4	65.1	Zr—O—Si
$3d_{5/2}$	B	183.1	34.9	Zr—OH

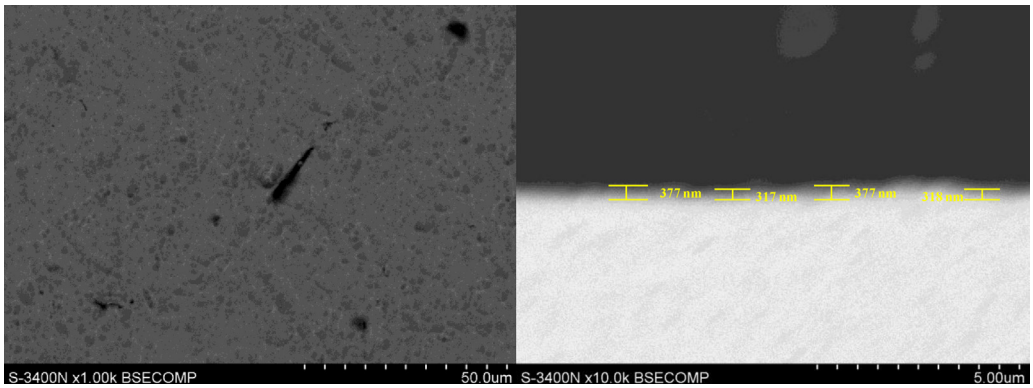

Fig. 3. The SEM image of the surface and the cross section of the oxide layer on the zirconium anodized at 100 V in 0.5 mol dm^{-3} K_2SiO_3 (Zr-ANO-0.5–100 sample).

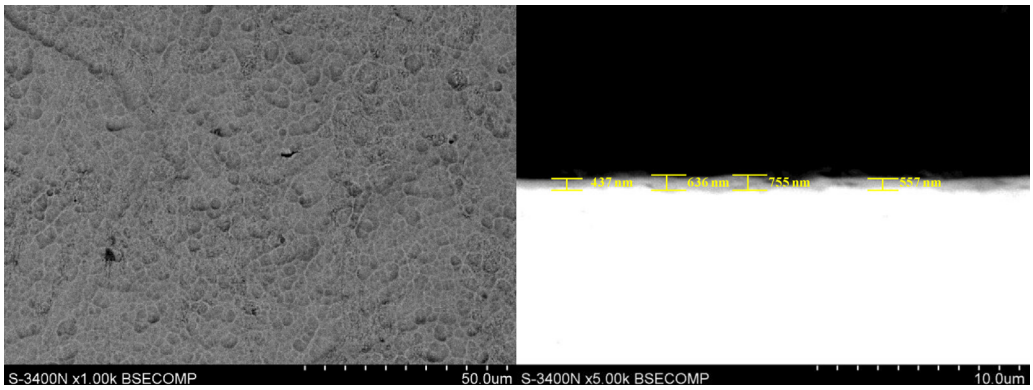

Fig. 4. The SEM image of the surface and the cross section of the oxide layer on the zirconium anodized at 200 V in 0.5 mol dm^{-3} K_2SiO_3 (Zr-ANO-0.5–200 sample).

1.0 mol dm^{-3}, respectively. The surface morphology of the Zr-ANO-0.1-400 sample after an oxidation at 400 V in a solution containing 0.1 mol dm^{-3} K_2SiO_3 is provided in Fig. 6. The color of the coating is light gray and characterized by numerous small pores with a diameter of less than 1 μm. The formed coating is characterized by a layered structure and with a thickness of 5.5 μm (Fig. 6). The cross-section shows that the coating is non-uniform and reveals numerous cracks, with the outer regions of the coating detached in several locations (Fig. 6). A layered nature of the coating is less apparent than the coatings formed on a Zircaloy-4 alloy in the sodium silicate solution [38,39]. A similar coating was formed during the anodization of Zircaloy-4 alloy in a solution containing only NaOH [40]. The peaks corresponding to the substrate metal as well as intense peaks for silicon, oxygen and potassium are observed in the EDX spectrum (Fig. 6). This finding indicates an appreciable incorporation of silicon and potassium into the oxide layer. According to the EDX point analysis of the layer, a distinct peak for zirconium and a small signal for oxygen are observed at the metal/oxide interface (Fig. 6). In contrast, more intense signal for oxygen and silicon is observed at another point near the surface. Marker studies indicate that the films are formed mainly at the metal/film interface due to the inward migration of oxygen ions. Hence, the cation transport number is low, approximately 0.05 [41]. In the case of the PEO treatment, silicon species were found at a relatively high concentration in the outer layer of the film with a thickness of approximately 20 nm. This region of the film may be formed by the outward migration of Zr^{4+} ions, possibly assisted by the precipitation of silica due to the reduction of the pH near the surface of the film during the anodic segment of the current cycle [42]. In the pre-sparking stage of the treatment, silicon is a minor component of the main film [36,38]. In the case of anodization in a solution containing 0.5 mol dm^{-3} K_2SiO_3, the formed coating was characterized by a considerable surface development as well as large pores with a diameter of up to 20 μm (Zr-ANO-0.5-400 sample; Fig. 7). The Zr/Si atomic ratio decreased substantially, to a value of 0.085 (Table 1). These results reveal a significant amount of silicon in the coating. The analysis of the high resolution spectra of O 1s, Si 2p, and Zr 3d was performed for Zr-ANO-0.5-400 sample (Fig. 8). The XPS measurements allowed determination of the Si/Zr and Si/O (excluding oxygen from adsorbed organic contaminants) atomic ratios as 2.07 and 0.48. These indicated that the surface layer is composed of silica-like species. The high resolution XP spectra were deconvoluted into minimum number of components and the resulting data were summarized in Table 2 and provide a comparison of the electronic states of elements at the surface studied. The assignment of components was performed using

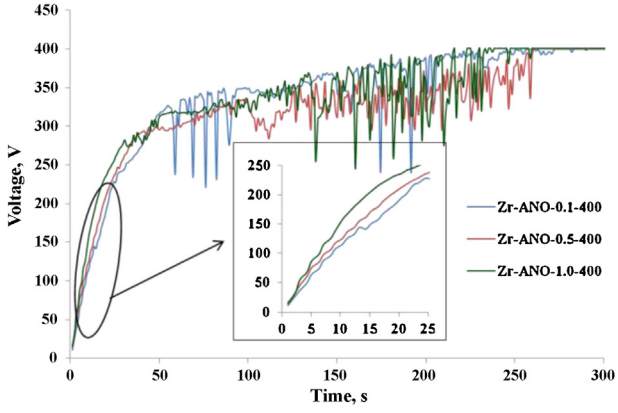

Fig. 5. The voltage–time responses for the zirconium samples anodized at 400 V in solutions with different concentration of K_2SiO_3 (Zr-ANO-x-400 samples).

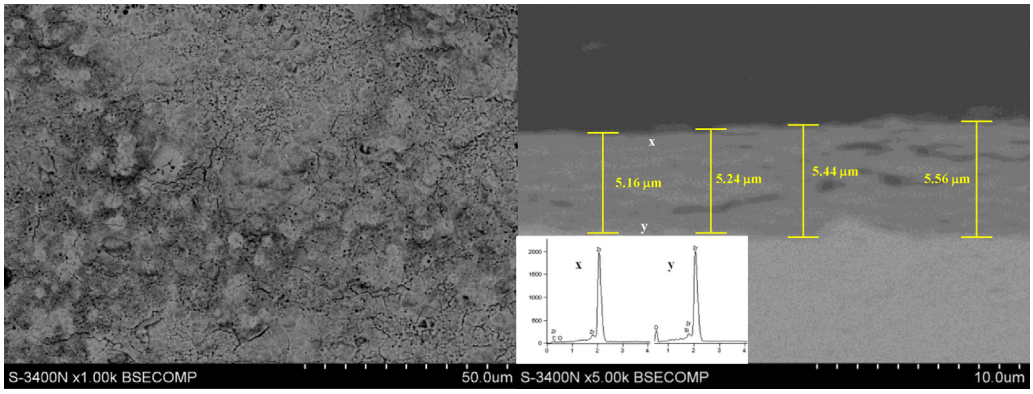

Fig. 6. The SEM image of the surface, the cross section, and the EDX point analysis (x and y points on the right image) of the oxide layer on the zirconium anodized at 400 V in 0.1 mol dm^{-3} K_2SiO_3 (Zr-ANO-0.1–400 sample).

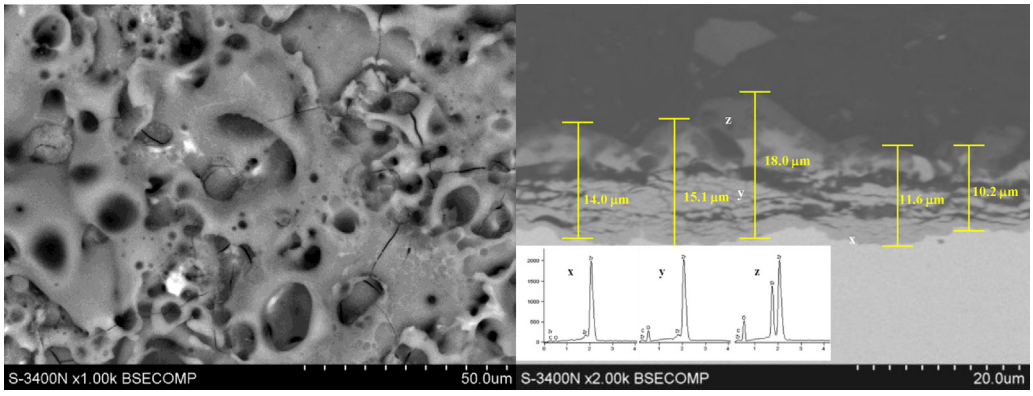

Fig. 7. The SEM image of the surface, the cross section, and the EDX point analysis (x, y, and z points on the right image) of the oxide layer on the zirconium anodized at 400 V in 0.5 mol dm^{-3} K_2SiO_3 (Zr-ANO-0.5–400 sample).

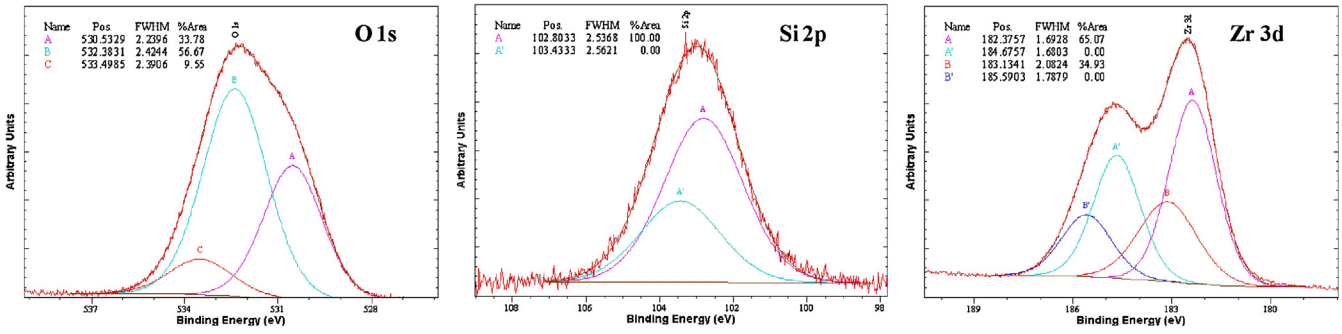

Fig. 8. Deconvoluted spectra of O 1s, Si 2p, and, Zr 3d core excitations for the zirconium anodized at 400 V in 0.5 mol dm^{-3} K_2SiO_3 (Zr-ANO-0.5-400 sample).

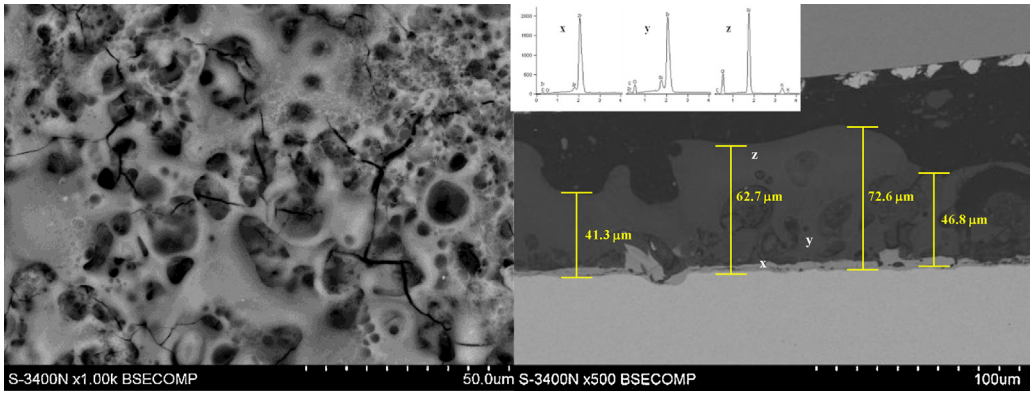

Fig. 9. The SEM image of the surface, the cross section, and the EDX point analysis (x, y, and z points on the right image) of the oxide layer on the zirconium anodized at 400 V in 1.0 mol dm^{-3} K_2SiO_3 (Zr-ANO-1.0-400 sample).

standard databases [43–45]. The O 1s spectrum was de-convoluted into three components wherein the most intensive component (B) was assigned to the oxygen bonded to the silicon (silicates and/or silica) and the second component (A) was assigned to the oxygen in the metal oxides, and lowest (C) to oxygen in adsorbed water and organic contaminants. Analysis of Si 2p spectrum revealed single doublet (A) at Si $2p_{3/2}$ BE of 102.8 eV assigned to Si^{4+} in silicates or amorphous silica [43–45]. The relatively broad Si $2p_{3/2}$ component of full width at half maximum of 2.5 eV suggests relatively large variety of possible surroundings of silicon cation although all related to silicates. The Zr 3d core excitation was deconvoluted into two components i.e. the major one (A) to Zr^{4+} in zirconium silicate and the minor one (B) also to Zr^{4+} but in more electronegative surrounding like in zirconium hydroxide [45,46]. Additionally, little amount (3.4 at.%) of potassium was found as silicate (K $2p_{3/2}$ of 293.7 eV) at the studied surface. Carbon contamination from the atmosphere is always present in surfaces exposed to air.

The cross-sectional analysis of Zr-ANO-0.5-400 specimen also exhibited the stratification of the fabricated coating, as shown in Fig. 7. Point EDX analysis at the metal/oxide boundary mainly indicated the presence of zirconium (Fig. 7). The signals for oxides became more intense as the distance from the surface decreased. Moreover, a very intense silicon peak is observed right at the surface. In this case, the thickness of the formed coating was between 10 and 18 μm. Increasing the K_2SiO_3 concentration from 0.5 to 1.0 did not cause a significant change in the surface of the anodized samples (Zr-ANO-1.0–400 sample; Fig. 9). However, the produced coating appeared more cracked. The Zr/Si atomic ratio was 0.005, indicating a total coverage of the surface with silicate or silica (Table 2). The cross-sectional image (Fig. 9) reveals that the thickness of the oxide layer was between 41 and 71 μm with many connecting holes. The growth of an oxide layer by anodic oxidation and local breakdown with a small spark, as well as the subsequent oxygen gas evolution resulted in the formation of this complicated structure [46,47]. The EDX point cross-sectional analysis of Zr-ANO-1.0-400 sample is provided in Fig. 9. As observed with the previous specimen, the coating exhibited a laminar character. Only peaks for Si, O, and K were observed at the surface of the coating. This finding reveals the presence of potassium silicate and silica on the surface of the sample.

The temperature in the discharge area can be up to several thousand degrees Celsius [11], leading to the local evaporation of the solution, the crystallization of components and, finally, the incorporation of components into the oxide layer. Another feature of plasma electrolysis is the formation of specific surface structures, such as metastable high temperature phases, non-equilibrium solid solutions, mixed-compounds, glassy phases, and other characteristics. These substances are formed as a result of plasma thermochemical reactions at the surface of the electrode [11]. The incorporation of anions from the anodizing electrolyte into the oxide film is strongly affected by the nature of the electrolyte. For instance, organic acids anions are less incorporated into the oxide film due to the larger size of the alkyl chain compared with that of typical inorganic anions. In contrast, a significant amount of phosphate species (typically, a few at%) are incorporated into the growing film during the anodization in phosphate-based electrolytes [48]. In addition to the nature of the electrolyte, the process voltage fundamentally influences the possibility that elements will be incorporated into the oxide layer of titanium alloys. Because the voltage range of 100–200 V is lower than the breakdown voltage of the passive layer, no plasma oxidation was observed that resulted in a substantial incorporation of components in the oxide film. When a voltage of 400 V is used, silicon is incorporated in the oxide layer of zirconium (Zr-ANO-x-400 samples).

The open-circuit potential E_{OCP} of zirconium samples was recorded over a period of 1 h in the presence of Ringer's simulated body fluid. The E_{OCP} was found to increase as the specimen was etched in samples that were anodized at 400 V (Fig. 10). Such behavior indicates the formation of an oxide layer on the surface of the sample in Ringer's solution or the sealing of the existing layer on the surface of Zr [24,49,50]. In the case of samples that were oxidized at 100 and 200 V, the E_{OCP} slightly decreased before stabilizing (Fig. 10). This effect on E_{OCP} may demonstrate a certain activity of the samples in a physiological solution. These observations may result due to a change in the degree of crystallinity of the coating, the conversion of anhydrous oxides to hydrated oxides or the unsealing of the coating. Moreover, a very slow dissolution of the oxides in the Ringer's solution is also possible [51,52]:

$$ZrO_2 + 2H^+ \rightarrow H_2O + ZrO^{2+} \quad (2)$$

The highest E_{OCP} values after 60 min of incubation in Ringer's physiological solution were obtained for specimen that were oxidized at 100 V.

The cyclic polarization curves (CV) obtained for zirconium samples in Ringer's solution are provided in Fig. 11. The polarization curve obtained for pure Zr is similar to that of zirconium at a pH 8 buffer containing chlorides [53]. With increasing potential, the rate of hydrogen evolution decreases and the oxidation of zirconium begins, resulting in passivation due to the formation of a zirconium oxide film. At 302 mV, the slope in the CV plot starts to increase sharply (Fig. 11). In this region, the breakdown of the passive film and oxygen evolution at higher potentials contributes to the measured current. Following a further increase in the potential, the current density increases very sharply. This effect is due to the accelerated anodic dissolution caused by the breakdown of the passive layer and the eventual oxygen evolution. According to literature, in acidic solutions, severe anodic dissolution induced either by the flaking of zirconium oxide from the surface or the weakening of the oxide film by H_3O^+ ions produces a porous ZrO_2 film [53,54]. However, in basic solutions, the mechanism of passive film breakdown is expected to be different. The passive property of the film can be changed due to loss of water from the structure [55]. In the case of Zr-ANO-0.5-100 and Zr-ANO-0.5-200 zirconium samples, the breakdown potential (E_{BREAK}) was 1440 and 1940 mV, respectively (Table 3). However, the current density was significantly lower in comparison with pure zirconium (Fig. 11). This behavior in Ringer's solution is associated with a passive layer of several hundred nanometers in thickness, formed on the surface, which protects the metal against corrosion. The zirconium anodized at a voltage of 400 V completely changed the shape of the CV curves, regardless of the solution used. Until 3 V, the breakdown potential was not observed and the recorded current density did not exceed a few mA cm^{-2} (Fig. 11). This behavior of Zr-ANO-x-400 samples is typical of zirconium alloys after PEO and clearly confirms its excellent corrosion resistance [47].

Fig. 12 provides the potentiodynamic polarization curves of pure zirconium and anodized samples. The corrosion current density (i_{CORR}), corrosion potential (E_{CORR}), and polarization resistance (R_p) obtained by the linear polarization method are summarized in Table 3. The corrosion potential of the Zr substrate is −340 mV and its corrosion current density is 234.68×10^{-9} A cm^{-2}. In addition, the polarization resistance is 92.63×10^3 Ω cm^2. The anodizing of zirconium samples at 100 and 200 V results in a significant shift in the corrosion potential toward the anodic side to 4.58 and −40.3 mV, respectively. The corrosion current density decreases considerably: Zr-ANO-0.5-100 with 2.54×10^{-9} A cm^{-2} and Zr-ANO-0.5-200 with 6.37×10^{-9} A cm^{-2}. In contrast, the polarization resistance increases to 8.54×10^6 Ω cm^2 and 3.41×10^6 Ω cm^2, respectively. The use of a voltage higher than the passive layer breakdown potential causes an increase in the corrosion resistance in comparison to pure zirconium (Fig. 12; Table 3). The corrosion potential increases with decreasing K_2SiO_3 content in the

Table 3
The results of corrosion resistance investigations of the zirconium in Ringer's solution.

Sample	K_2SiO_3, mol dm^{-3}	U, V	E_{CORR}, mV	R_p, Ω cm^2	i_{CORR}, A cm^{-2}	E_{BREAK}, mV
Zr	–	–	−34,058	92.6×10^3	2347×10^{-9}	302
Zr-ANO-0.5-100	0.5	100	4.58	8.5×10^6	2.5×10^{-9}	1441
Zr-ANO-0.5-200		200	−40.3	3.4×10^6	6.4×10^{-9}	1940
Zr-ANO-0.5-400		400	−27,919	1205×10^3	1804×10^{-9}	–
Zr-ANO-0.1-400	0.1	400	−15,820	3378×10^3	64.4×10^{-9}	–
Zr-ANO-1.0-400	1.0		−30,525	2336×10^3	93.1×10^{-9}	–

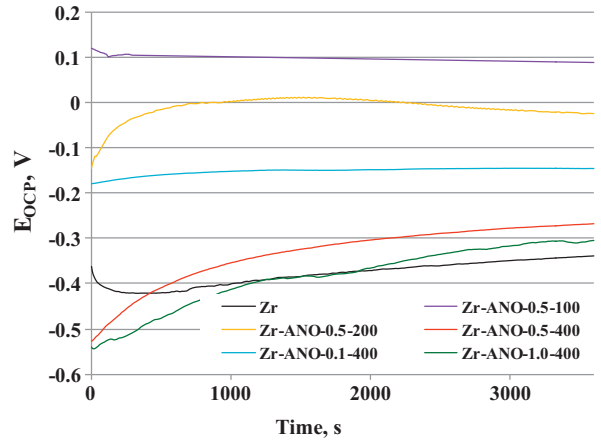

Fig. 10. The variation of the E_{OCP} with time for the etched zirconium and zirconium anodized at different conditions (Zr-ANO-x-y samples) in Ringer's solution.

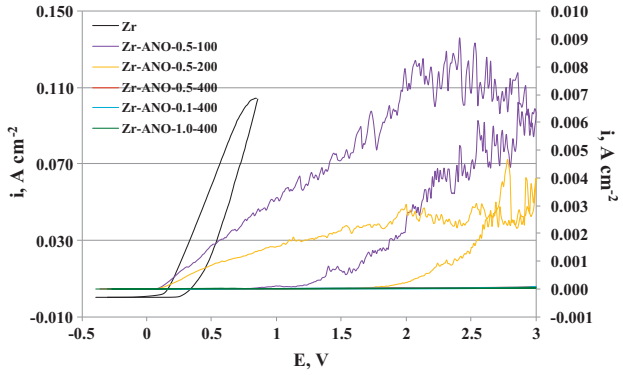

Fig. 11. The cyclic polarization curves recorded for the etched zirconium (left axis) and zirconium anodized at different conditions (Zr-ANO-x-y samples; right axis).

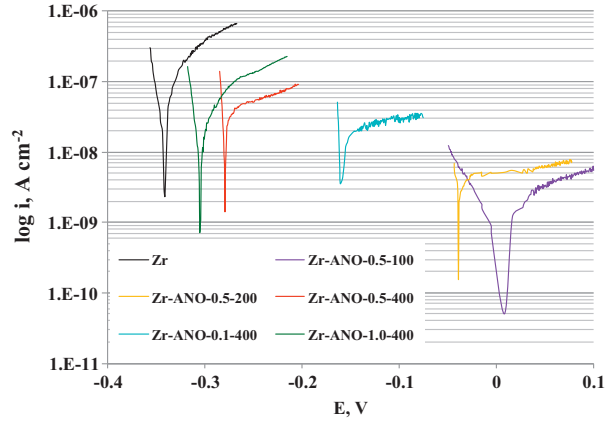

Fig. 12. The polarization curves recorded for the etched zirconium and zirconium anodized at different conditions (Zr-ANO-x-y samples).

anodization bath, which is associated with the structure and thickness of the formed passive layer. Moreover, the corrosion current density of Zr-ANO-x-400 specimens is lower than of pure zirconium (Fig. 12), and the polarization resistance increases (Table 3). A dense barrier layer with a thickness of 200–600 nm at the PEO coating/Zr plays an important role in the corrosion properties of coated samples. This barrier layer may be discerned in Figs. 6, 7 and 9. Moreover, the thick coating with high hardness and elastic modulus is relatively brittle, which might result in the presence of several cracks [47]. Thus, Cl^- ions in the NaCl solution can easily penetrate into the coating along these cracks. A suitable coating thickness should be selected to obtain anti-corrosion coatings using the PEO process on Zr. Because the degradation of Zr often takes place though Zr, it is easy to form a protective passive film. As shown in Fig. 11, the breakdown potential (E_{BREAK}) of Zr for pitting attack is 302 mV, but the potential of coated alloys is greatly improved to over +3 V for samples anodized at 400 V. Hence, the PEO coating on Zr has excellent pitting corrosion resistance.

4. Conclusions

This work represents a study on the incorporation of silicon into an oxide film in zirconium using the anodic oxidation method. The process was performed in a solution containing K_2SiO_3 and KOH. The incorporation of a significant amount of silicon was observed upon applying a potential above the breakdown voltage of the oxide layer, namely 400 V. Moreover, the amount of the incorporated silicon increases with increasing potassium silicate concentration in the anodizing solution. The silicon incorporated into the oxide coating on zirconium occurs in the form of silica and silicates. This type of incorporation of Si into the oxide layer can be favorable for the adsorption of specific ions and for following the crystallization of hydroxyapatite in a tissue environment. Anodic oxidation of zirconium leads to a significant improvement in the corrosion resistance of the material in the presence of Ringer's physiological solution. The produced oxide layers require further investigation (biocorrosion and bioactivity), the results of which will be presented in next study.

Acknowledgements

This work was supported by the Polish Ministry of Science and Education under research project no. IP 2011 0494 71.

References

[1] W. Simka, M. Kaczmarek, A. Baron-Wiecheć, G. Nawrat, J. Marciniak, J. Żak, Electropolishing and passivation of NiTi shape memory alloy, Electrochimica Acta 55 (2010) 2437.
[2] T. Hryniewicz, K. Rokosz, J. Valicek, R. Rokicki, Effect of magnetoelectropolishing on nanohardness and Young's modulus of titanium biomaterial, Materials Letters 83 (2012) 69.
[3] T. Hryniewicz, P. Konarski, R. Rokicki, J. Valicek, SIMS studies of titanium biomaterial hydrogenation after magnetoelectropolishing, Surface and Coatings Technology 206 (2012) 4027.
[4] P.C. Rath, L. Besra, B.P. Singh, S. Bhattacharjee, Titania/hydroxyapatite bi-layer coating on Ti metal by electrophoretic deposition: characterization and corrosion studies, Ceramics International 38 (2012) 3209.

[5] D.J. Blackwood, K.H.W. Seah, Electrochemical cathodic deposition of hydroxyapatite: Improvements in adhesion and crystallinity, Materials Science and Engineering C 29 (2009) 1233.
[6] F. Muratore, A. Baron-Wiechec, A. Gholinia, T. Hashimoto, P. Skeldon, G.E. Thompson, Comparison of nanotube formation on zirconium in fluoride/glycerol electrolytes at different anodizing potentials, Electrochimica Acta 58 (2011) 389.
[7] G.D. Sulka, A. Brzózka, L. Liu, Fabrication of diameter-modulated and ultrathin porous nanowires in anodic aluminum oxide templates, Electrochimica Acta 56 (2011) 4972.
[8] J. Szewczenko, J. Marciniak, Tyrlik-Held J., K. Nowinska, Effect of surface pretreatment on corrosion resistance of anodically oxidized Ti6Al7Nb alloy, Lecture Notes in Computer Science 7339 (2012) 398.
[9] J. Szewczenko, M. Pochrzast, W. Walke, Evaluation of electrochemical properties of modified Ti-6Al-4V ELI alloy, Przeglad Elektrotechniczny 87 (2011) 177.
[10] J. Szewczenko, W. Walke, K. Nowinska, J. Marciniak, Corrosion resistance of Ti-6Al-4V alloy after diverse surface treatments, Materialwissenschaft und Werkstofftechnik 41 (2010) 360.
[11] A.L. Yerokhin, X. Nie, A. Leyland, A. Matthews, S.J. Dowey, Plasma electrolysis for surface engineering, Surface and Coatings Technology 122 (1999) 73.
[12] W. Simka, A. Sadkowski, M. Warczak, A. Iwaniak, G. Dercz, J. Michalska, A. Maciej, Characterization of passive films formed on titanium during anodic oxidation, Electrochimica Acta 56 (2011) 8962.
[13] A. Strzała, W. Simka, M. Marszałek, Hydrothermal synthesis of hydroxyapatite on titanium after anodic oxidation, Acta Physica Polonica A 121 (2012) 561.
[14] W. Simka, A. Iwaniak, G. Nawrat, A. Maciej, J. Michalska, K. Radwański, J. Gazdowicz, Modification of titanium oxide layer by calcium and phosphorus, Electrochimica Acta 54 (2009) 6983.
[15] W. Simka, Preliminary investigations on the anodic oxidation of Ti-13Nb-13Zr alloy in a solution containing calcium and phosphorus, Electrochimica Acta 56 (2011) 9831.
[16] A. Krzakała, et al., Formation of bioactive coatings on a Ti–6Al–7Nb alloy by plasma electrolytic oxidation, Electrochimica Acta (2012) http://dx.doi.org/10.1016/j.electacta.2012.07.075
[17] M. Geetha, A.K. Singh, R. Asokamani, A.K. Gogia, Plasma electrolysis for surface engineering, Progress in Materials Science 54 (2009) 397.
[18] S. Nag, R. Banerjee, H.L. Fraser, Microstructural evolution and strengthening mechanisms in Ti–Nb–Zr–Ta, Ti–Mo–Zr–Fe and Ti–15Mo biocompatible alloys, Materials Science and Engineering C 25 (2005) 357.
[19] K.L. Wapner, Implications of metallic corrosion in total knee arthroplasty, Clinical Orthopaedics and Related Research 271 (1991) 12.
[20] E. Eisenbarth, D. Velten, M. Muller, R. Thull, J. Breme, Biocompatibility of β-stabilizing elements of titanium alloys, Biomaterials 25 (2004) 5705.
[21] P.D. Miller, J.W. Holladay, Friction and wear properties of titanium, Wear 2 (1958) 133.
[22] P.G. Liang, E.S. Ferguson, E.S. Hodge, Tissue reaction in rabbit muscle exposed to metallic implants, Journal of Biomedical Materials Research 1 (1967) 135.
[23] S.L. Assis, S. Wolynec, I. Costa, Corrosion characterization of titanium alloys by electrochemical techniques, Electrochimica Acta 51 (2006) 1815.
[24] N.T.C. Oliveira, E.A. Ferreira, L.T. Duarte, S.R. Biaggio, R.C. Rocha-Filho, N. Bocchi, Corrosion resistance of anodic oxides on the Ti–50Zr and Ti–13Nb–13Zr alloys, Electrochimica Acta 51 (2006) 2068.
[25] S.Y. Yu, J.R. Scully, Corrosion and passivity of Ti-13% Nb-13% Zr in comparison to other biomedical implant alloys, Corrosion 53 (1997) 965.
[26] M.A. Khan, R.L. Williams, D.F. Williams, The corrosion behaviour of Ti–6Al–4V, Ti–6Al–7Nb and Ti–13Nb–13Zr in protein solutions, Biomaterials 20 (1999) 631.
[27] S.L. Assis, I. Costa, Electrochemical evaluation of Ti-13Nb-13Zr, Ti-6Al-4V and Ti-6Al-7Nb alloys for biomedical application by long-term immersion tests, Materials and Corrosion 58 (2007) 329.
[28] W.Y. Guo, J. Sun, J.S. Wu, Electrochemical and XPS studies of corrosion behavior of Ti–23Nb–0.7Ta–2Zr–O alloy in Ringer's solution, Materials Chemistry and Physics 113 (2009) 816.
[29] Y.L. Zhou, M. Niinomi, T. Akahori, H. Fukui, H. Toda, Corrosion resistance and biocompatibility of Ti–Ta alloys for biomedical applications, Materials Science and Engineering A 398 (2005) 28.
[30] S.D. Puckett, E. Taylor, T. Raimondo, T.J. Webster, The relationship between the nanostructure of titanium surfaces and bacterial attachment, Biomaterials 31 (2010) 706.
[31] P. Huang, K.W. Xu, Y. Han, Preparation and apatite layer formation of plasma electrolytic oxidation film on titanium for biomedical application, Materials Letters 59 (2005) 185.
[32] H. Hu, X. Liu, Ch Ding, Preparation and cytocompatibility of Si-incorporated nanostructured TiO_2 coating, Surface and Coatings Technology 204 (2010) 3265.
[33] A.M. Pietak, J.W. Reid, M.J. Stott, M. Sayer, Silicon substitution in the calcium phosphate bioceramics, Biomaterials 28 (2007) 4023.
[34] E. Carlisle, Silicon: an essential element for the chick, Science 178 (1972) 619.
[35] T. Gao, H.T. Aro, H. Ylanen, E. Vuorio, Silica-based bioactive glasses modulate expression of bone morphogenetic protein-2 mRNA in Saos-2 osteoblasts in vitro, Biomaterials 22 (2001) 1475.
[36] E. Matykina, R. Arrabal, P. Skeldon, G.E. Thompson, P. Wang, P. Wood, Plasma electrolytic oxidation of a zirconium alloy under AC conditions, Surface and Coatings Technology 204 (2010) 2142.
[37] F.S. Cheng, D. Wei, Y. Zhou, H. Guo, Characterization and properties of microarc oxidized coatings containing Si, Ca and Na on titanium, Ceramics International 37 (2011) 1761.
[38] Y. Cheng, E. Matykina, P. Skeldon, G. Thompson, Characterization of plasma electrolytic oxidation coatings on Zircaloy-4 formed in different electrolytes with AC current regime, Electrochimica Acta 56 (2011) 8467.
[39] Y. Cheng, E. Matykina, R. Arrabal, P. Skeldon, G. Thompson, Plasma electrolytic oxidation and corrosion protection of Zircaloy-4, Surface and Coatings Technology 206 (2012) 3230.
[40] J. Li, X. Bai, D. Zhang, H. Li, Characterization and structure study of the anodic oxide film on Zircaloy-4 synthesized using NaOH electrolytes at room temperature, Applied Surface Science 252 (2006) 7436.
[41] J.A. Davies, B. Domeij, J.P.S. Pringle, F. Brown, W.D. Mackintosh, The migration of metal and oxygen during anodic film formation, Journal of the Electrochemical Society 112 (1965) 675.
[42] F. Monfort, A. Berkani, E. Matykina, P. Skeldon, G.E. Thompson, H. Habazaki, K. Shimizu, Development of anodic coatings on aluminium under sparking conditions in silicate electrolyte, Corrosion Science 49 (2007) 672.
[43] J.F. Moulder, W.F. Stickle, P.E. Sobol, K. Bomben, Handbook of X-ray Photoelectron Spectroscopy, 2nd ed., Perkin-Elmer Corporation (Physical Electronics), 1992.
[44] Electron Spectroscopy Database. www.lasurface.com
[45] NIST X-ray Photoelectron Spectroscopy Database. http://srdata.nist.gov/xps/
[46] J.Y. Ha, Y. Tsutsumi, H. Doi, N. Nomura, K.H. Kim, T. Hanawa, Enhancement of calcium phosphate formation on zirconium by micro-arc oxidation and chemical treatments, Surface and Coatings Technology 205 (2011) 4948.
[47] W. Xue, Q. Zhu, Q. Jin, M. Hua, Characterization of ceramic coatings fabricated on zirconium alloy by plasma electrolytic oxidation in silicate electrolyte, Materials Chemistry and Physics 120 (2010) 656.
[48] R. Narayanan, S.K. Seshadri, Point defect model and corrosion of anodic oxide coatings on Ti–6Al–4V, Corrosion Science 50 (2008) 1521.
[49] A. Robin, O.A.S. Carvalho, S.G. Schneider, S. Schneider, Corrosion behavior of Ti-xNb-13Zr alloys in Ringer's solution, Materials and Corrosion 59 (2008) 929.
[50] M.R. Souto, M.M. Laz, R.L. Reis, Degradation characteristics of hydroxyapatite coatings on orthopaedic TiAlV in simulated physiological media investigated by electrochemical impedance spectroscopy, Biomaterials 24 (2003) 4213.
[51] M. Pourbaix, Atlas of Electrochemical Equilibria in Aqueous Solutions, second ed., Nace, Houston, 1974.
[52] D.J. Blackwood, L.M. Peter, D.E. Williams, Stability and open circuit breakdown of the passive oxide film on titanium, Electrochimica Acta 33 (1988) 1143.
[53] A. Mamun, R. Schennach, J.R. Parga, M.Y.A. Mollah, M.A. Hossain, D.L. Cocke, Passive film breakdown during anodic oxidation of zirconium in pH 8 buffer containing chloride and sulfate, Electrochimica Acta 46 (2001) 3343.
[54] P. Meisterjahn, H.W. Hoppe, J.W. Schultze, Electrochemical and XPS measurements on thin oxide films on zirconium, Journal of Electroanalytical Chemistry 217 (1987) 159.
[55] P. Southworth, A. Hamnett, A.M. Riley, J.M. Sykes, An ellipsometric and rrde study of iron passivation and depassivation in carbonate buffer, Corrosion Science 28 (1988) 1139.